AIP | Journal of Applied Physics

Quantum dot energy levels and spectrum for different geometries

C. Tablero

Citation: J. Appl. Phys. **106**, 074306 (2009); doi: 10.1063/1.3243290
View online: http://dx.doi.org/10.1063/1.3243290
View Table of Contents: http://jap.aip.org/resource/1/JAPIAU/v106/i7
Published by the AIP Publishing LLC.

Additional information on J. Appl. Phys.

Journal Homepage: http://jap.aip.org/
Journal Information: http://jap.aip.org/about/about_the_journal
Top downloads: http://jap.aip.org/features/most_downloaded
Information for Authors: http://jap.aip.org/authors

ADVERTISEMENT

Downloaded 26 Jun 2013 to 128.42.202.150. This article is copyrighted as indicated in the abstract. Reuse of AIP content is subject to the terms at: http://jap.aip.org/about/rights_and_permissions

Quantum dot energy levels and spectrum for different geometries

C. Tablero[a)]
Instituto de Energía Solar, Universidad Politécnica de Madrid, Ciudad Universitaria s/n, 28040 Madrid, Spain

(Received 12 June 2009; accepted 9 September 2009; published online 13 October 2009)

The dispersion in the dot size, shape, and composition leads to a difficult comparison with experimental spectroscopy and transport data even if the growth conditions are similar. In this work, an extensive analysis of the influence of the dot size and shape on the electron and hole energy states and on transition energies is carried out using a unified model of the semiconductor band structure. In this study we obtain the electron energy spectra for three-dimensional small InAs/GaAs quantum dots of several different truncated shapes described in the literature: tetrahedral, pyramidal with base of different geometry, etc. Also, in order to give an idea of the flexibility of the method, the icosahedral geometry is analyzed. The combination of theoretical results using a unified model for all the geometries with structural techniques will allow a more precise analysis of experimental samples. © *2009 American Institute of Physics*. [doi:10.1063/1.3243290]

I. INTRODUCTION

Semiconductor quantum dots (QDs) have recently become of great interest because of the electronic characteristics and the possibility of manufacturing realistic QDs in laboratories by applying nanotechnology. The electronic states in QD manifest localization: the particles are confined and stationary in the three spatial dimensions and have discrete energy levels like those of a single atom. These electronic characteristics make it possible to model atomic physics in macroscopic systems both experimentally and theoretically. By combining miniaturization and single electron control (charge or spin), QDs are promising candidates for active material in novel optoelectronic devices, QD Lasers, QD infrared photodetector, single-photon emitters, quantum cryptography, etc. In fact, a large part of the intensive experimental and theoretical investigation is driven by the prospect of manufacturing a new generation of electronic and photonic devices (QD lasers and solar cells, for instance). The studies of semiconductor QD have focused on both experimental and theoretical aspects.

Experiments indicate that QDs can have several shapes depending on the manufacturing methodology, such as disk, ellipsoid, conical, pyramidal, tetrahedral, or an islandlike shape. Nevertheless, even if the methodology is the same, the experimental results demonstrate that the geometry of QD is not precise. In the case of pyramidal QD[1,2] they are formed spontaneously, e.g., via strain-driven Stransky–Krastanow growth or colloidal nucleation. Under such growth conditions, the QDs are positioned randomly and their size exhibits a very large dispersion. There is evidence that the InAs/GaAs QDs are pyramidal[3,4] although possibly truncated[5] or lens shaped.[6–8] Neither the different shapes of the QD nor the facet orientation are clear. Therefore, unfortunately, no consistent description of the dot shape can be drawn from the literature because of the different conditions used in the dot formation. Moreover, some works have suggested that the material composition may not be uniform.[9]

This dispersion in the dot size, shape, and composition produces an energy fluctuation in the strong confinement region. The spectral broadening caused is the major concerns in the practical laser and optical applications. Therefore, a direct comparison of calculated energy levels for a given size and shape with experimental spectroscopy and transport data is difficult.

Theoretically, in order to model the QD electronic properties, the effective mass approximation, the multiband *kp* method and the pseudopotential method have been used. Most models use numerical methods with a high computational cost which depend on the theoretical scheme used and on the QD size and shape. While large-scale calculations using complicated Hamiltonians have become feasible, the results are no better than those using the input parameters and dot shape models. For instance, the multielectron interaction and other factors in small QDs generally affect the electron energy in the order of a few meV. But, at the same time, the variations in the dot size and shape can produce an energy change up to an order of 0.1 eV in the strong confinement region. A wide range of shapes and sizes have been used in the theoretical models to simulate InAs/GaAs dot properties. The commonly used shapes include disk,[10] lens,[11] cone,[12] spherical,[13] pyramidal,[14] and cubic[15] shapes were also used. However, a comprehensive analysis of the influence of the dot size and shape on the electron energy states by using a unified model of the semiconductor band structure has not yet been carried out. Different models are usually used for different geometries.

For all of the aforementioned, the dispersion in the dot size and shape leads to a difficult comparison with experimental spectroscopy and transport data. Experimentally, it will be very useful to have an extensive and direct relationship between the calculated energy levels for a given size and shape. In this way, it would be promising to carry out inverse engineering. From an extensive relationship of levels from the theoretical results, together with the experimental

[a)]Electronic mail: ctablero@etsit.upm.es.

 © 2009 American Institute of Physics

Downloaded 26 Jun 2013 to 128.42.202.150. This article is copyrighted as indicated in the abstract. Reuse of AIP content is subject to the terms at: http://jap.aip.org/about/rights_and_permissions

results of possible geometries, we would be able to induce the size, the shape, and the proportion of the geometries of the possible QD in the experimental samples. To do so, it is necessary to use a unified model for all the possible geometries.

Therefore, the goal of this work is to provide extensive information on QD energy levels as a function of the most common geometries, using a unified theoretical model for all the geometries.[16] The results of this model compare well with experimental and theoretical results in the literature. For instance, lens-shaped InAs/GaAs QD with height of 2.5 nm and base of 20 nm has electron and hole confinement energies of 0.23 and 0.19 eV.[17] These results have been obtained using atomistic pseudopotential plus configuration interaction calculations. With the model used in this work these electron and hole confinement energies are 0.24 and 0.20 eV, respectively. The ground and first electron confined energies, with respect to the potential barrier, for a lens-shaped strained InAs/GaAs QD with height of 3.5 nm and diameter of 25 nm are approximately −0.3 and −0.2 eV.[18] The energies have been calculated by a multiband, multivalley, pseudopotential with a basis set of strain-dependent linear combination of bulk bands. These energies are reproduced with the model used in this work.

Of course, there are many possible QD geometries and barrier materials. In this study we calculate and compare the electron energy spectra for three-dimensional small InAs/GaAs QDs of several different shapes. Most of them described in the literature are with (truncated) pyramidal and with (truncated) tetrahedral shapes. Additionally, we have analyzed QD with icosahedral geometry. Apart from the spherical symmetry, the icosahedron group has the highest symmetry possible for a three-dimensional object. This choice is to illustrate the flexibility of the methodology used with respect to the shape of the QD.

II. RESULTS AND DISCUSSION

The theoretical model used is described in Ref. 16. This model is based in the effective mass approximation. The strain, electron interactions, and spin orbit are not included in the model. The wave function for the QD system is expanded as a linear combination of a basis set. This basis set is made of the autofunctions of a problem with hard boundary conditions. Then, the Schrödinger equation for a QD of arbitrary shape embeds into a barrier material (without hard boundary conditions) is solve using the symmetry properties of the system. This model is characterized mainly by two properties: (i) is valid for arbitrarily shaped QD and (ii) in this model is used the symmetry, reducing the computational cost.

Firstly, we have carried out a test for the convergence and robustness of the method for each geometry analyzed. The results presented in this work are well converged with respect to size of the basis set. This size is proportional to n^3 (see Ref. 16). An increase in n from 15 to 25 leads to differences of $10^{-3}-10^{-4}$ eV in the ground state for all the cases analyzed.

The energy spectrum of the QD consists of a set of discrete levels classified according to the irreducible representations of the group. For the truncated pyramidal QD the groups are C_{3v} (triangular equilateral base), C_{4v} (square base), C_{5v} (pentagonal base), and C_{6v} (hexagonal base). For the tetrahedral QD the point group is T_d, and for the icosidodecahedron, an archimedean solid, is the icosahedral group I_h.

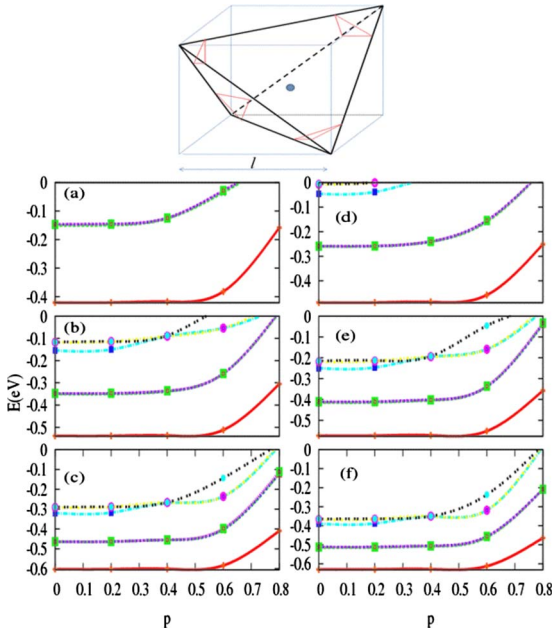

FIG. 1. (Color online) Energy of the ground and first electronic states (with respect to the potential barrier) for tetrahedral-shaped QD embedded in an cube of (a) 10 nm, (b) 12 nm, (c) 14 nm, (d) 16 nm, (e) 18 nm, and (f) 20 nm. p is the truncating parameter of the tetrahedral QD with $0 \leqslant p \leqslant 1$ ($p=0$ corresponds to the tetrahedron without truncation and $p=1$ correspond to the point in the center of the cube). In the upper panel the truncated tetrahedral QD is represented. The tetrahedron without truncation is imbedded in a cube of edge l. The tetrahedron is truncated by the planes perpendicular to the vectors from the origin to the vertices of the cube and that they contain the points $d(-1,1,1)$, $d(1,1,-1)$, $d(1,-1,1)$, $d(1,1,1)$, where $d=(1-p)\cdot l$.

A. Tetrahedral QD

The tetrahedron used is a polyhedron made up of four regular, or equilateral, triangular faces, three of which meet at each vertex (Fig. 1). The tetrahedron is imbedded in a cube with edge l. The tetrahedron edge is $\sqrt{2}$ times the cube edge l, i.e., $\sqrt{2}\cdot l$. However, the truncated tetrahedron has 4 regular hexagonal faces, 4 regular triangular faces, 12 vertices, and 18 edges. We have chosen the truncation percentage p, with $0 \leqslant p \leqslant 1$ as a parameter. For $p=0$ the tetrahedron is not truncated, whereas for $p=1$ is the point in the center of the cube.

There are some previous results on QD with a tetrahedral shape,[19–21] some of HgS/CdS QDs,[21] and others of InAs/GaAs.[19,20] For the InAs tetrahedral-shape QD in the GaAs matrix we have used the same parameters as in Refs. 19 and 20, i.e., 0.77 eV for the barrier potential $V_{B,e}$, $m_{\mathrm{QD},e}=0.028m_0$ for the QD effective mass and $m_{B,e}=0.067m_0$ for the barrier effective mass, where m_0 is the electron mass. The confined electron states for tetrahedral QD without truncation are analyzed in these references. In this work, the elec-

Downloaded 26 Jun 2013 to 128.42.202.150. This article is copyrighted as indicated in the abstract. Reuse of AIP content is subject to the terms at: http://jap.aip.org/about/rights_and_permissions

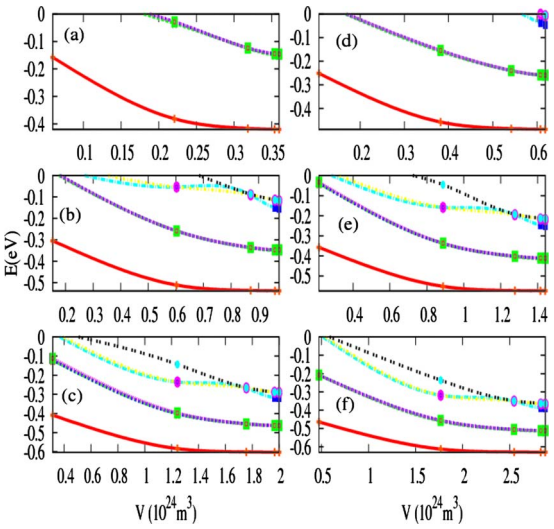

FIG. 2. (Color online) Energy of the firstly electronic states (with respect to the potential barrier) for a truncated tetrahedral-shaped QD embedded in an cube of (a) 10 nm, (b) 12 nm, (c) 14 nm, (d) 16 nm, (e) 18 nm, and (f) 20 nm as a function of the QD volume.

tronic and hole states for truncated tetrahedral QD have been analyzed as well. For holes the parameters used are $m_{B,h}=0.3774m_0$, and two different parametrizations in the literature for the barrier potential and QD effective mass: $V_{B,h}^{(G)}=0.316$ eV and $m_{\mathrm{QD},h}^{(G)}=0.34m_0$ (Ref. 22), and $V_{B,h}^{(C)}=0.266$ eV and $m_{\mathrm{QD},h}^{(C)}=0.59m_0$ (Ref. 23).

In Fig. 1 the confined states of the electrons are shown for different sizes of tetrahedral shape InAs/GaAs QD as a function of the truncation percentage p. As can be seen in the figure, the number of confined states decreases with the size and truncation percentage. The symmetry of the confined electronic states in ascending order of energy is $a_1, t_2, 2a_1, t_1, \ldots$. From the figure, the electronic states do not change appreciably between $0 \leqslant p \leqslant 0.45$. This is because the truncated portion has very little volume. The same electronic states are represented in Fig. 2, but now with respect to the volume of truncated tetrahedron. In this figure, the QDs with $0 \leqslant p \leqslant 0.45$ are localized very close for large volumes. On the other hand, for $p > 0.45$ the volume changes very quickly with p. From Figs. 1 and 2 it is interesting to note that for $l > 12$ nm and $p \sim 0.4$ there is a crossing between the third and fourth states.

In order to analyze the spectrum it is necessary know the selection rules, which depend on the symmetry. In Table I the allowed transitions for the point group of the QD analyzed in this work are indicated. In this table the representations (a_i, b_i), e_i, t_i, g, and h are uni-, bi-, tri-, tetra-, and pentadimensional, respectively. For this reason, for the group C_{2v} (pyramidal QD with rectangular base) the confined states are all not degenerates (a and b), for the C_{nv} with $n > 2$ they can be single or double degenerates (e), for the T_d there can additionally be triple degenerate states (t), the I can also have states tetra- (g) and pentadegenerates (h). Because of the section rules in Table I, the transition depends in the QD symmetry and the possibilities are many. The number of electronic confined states is lower than the number of hole confined states. As the number of confined states, for the same symmetry, depends on the QD size, the smaller QD will have fewer electronic states and they will determine the number of allowed transitions.

TABLE I. Allowed transitions for the QD with different symmetries. The second column indicates the irreducible representations (IR), denoted by Γ_i, of the point group. The allowed transitions are indicated as $\Gamma_i \overset{a}{\leftrightarrow} \Gamma_j$, where Γ_i and Γ_j are the IR of the allowed transitions and $a=x,y,z$ is the polarization.

Group	IR(Γ_i)	Allowed transitions
C_{2v}	a_1, a_2, b_1, b_2	$\Gamma_i \overset{z}{\leftrightarrow} \Gamma_i, a_1 \overset{x}{\leftrightarrow} b_1, a_2 \overset{x}{\leftrightarrow} b_2, a_1 \overset{y}{\leftrightarrow} b_2, a_2 \overset{y}{\leftrightarrow} b_1$
C_{3v}	a_1, a_2, e	$\Gamma_i \overset{z}{\leftrightarrow} \Gamma_i, \Gamma_i \overset{x,y}{\leftrightarrow} e$ with $i \neq e$
C_{4v}	a_1, a_2, b_1, b_2, e	$\Gamma_i \overset{z}{\leftrightarrow} \Gamma_i, \Gamma_i \overset{x,y}{\leftrightarrow} e$
C_{5v}	a_1, a_2, e_1, e_2	$\Gamma_i \overset{z}{\leftrightarrow} \Gamma_i (a_1, a_2) \overset{x,y}{\leftrightarrow} e_1, (e_1, e_2) \overset{x,y}{\leftrightarrow} e_2$
C_{6v}	$a_1, a_2, b_1, b_2, e_1, e_2$	$\Gamma_i \overset{z}{\leftrightarrow} \Gamma_i, (a_1, a_2) \overset{x,y}{\leftrightarrow} e_1, (b_1, b_2, e_1) \overset{x,y}{\leftrightarrow} e_2$
T_d	a_1, a_2, e, t_1, t_2	$a_1 \overset{x,y,z}{\leftrightarrow} t_2, a_2 \overset{x,y,z}{\leftrightarrow} t_1, (e, t_1) \overset{x,y,z}{\leftrightarrow} (t_1, t_2), t_2 \overset{x,y,z}{\leftrightarrow} t_2$
I	a_1, t_1, t_2, g, h	$a_1 \overset{x,y,z}{\leftrightarrow} t_1, t_1 \overset{x,y,z}{\leftrightarrow} (t_1, h), t_2 \overset{x,y,z}{\leftrightarrow} (g, h), g \overset{x,y,z}{\leftrightarrow} (g, h), h \overset{x,y,z}{\leftrightarrow} h$

For example, in Fig. 3 the allowed transitions of a truncated tetrahedron imbedded in a cube of edge 12 nm are shown. From Fig. 1, with $p > 0.75$ there is only a confined electronic state of a_1-symmetry. Therefore, the allowed transitions will be from this a_1-electronic-state to a hole state with t_2-symmetry: $a_1(e) \rightarrow t_2(h)$. In this case, the first t_2-hole state is the first excited state. The ground hole state is the a_1-symmetry. Therefore, according to the selection rules there are no transitions from ground electron state to ground hole state for $p > 0.75$. For $p < 0.75$ there is an additional transition from the first excited t_2-electron state to the ground a_1-hole state: $t_2(e) \rightarrow a_1(h)$.

B. Pyramidal QD

A shape usually present in the samples for InAs/GaAs is the truncated pyramid, in general, with a square base. For this reason, the QD geometry shown in the figures corresponds to a truncated pyramidal QD with square base. Nevertheless, the geometries analyzed have been a general trun-

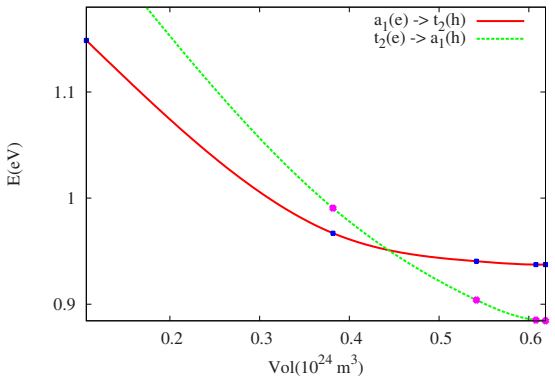

FIG. 3. (Color online) Energy of the first allowed transitions [$a_1(e) \rightarrow t_2(h)$ and $t_2(e) \rightarrow a_1(h)$, according to the Table I] for a truncated tetrahedral-shaped QD embedded in a cube of 12 nm as a function of the QD volume. For the hole levels the parametrization G has been used: $V_{B,h}^{(G)}=0.316$ eV and $m_{\mathrm{QD},h}^{(G)}=0.34m_0$ (Ref. 22).

Downloaded 26 Jun 2013 to 128.42.202.150. This article is copyrighted as indicated in the abstract. Reuse of AIP content is subject to the terms at: http://jap.aip.org/about/rights_and_permissions

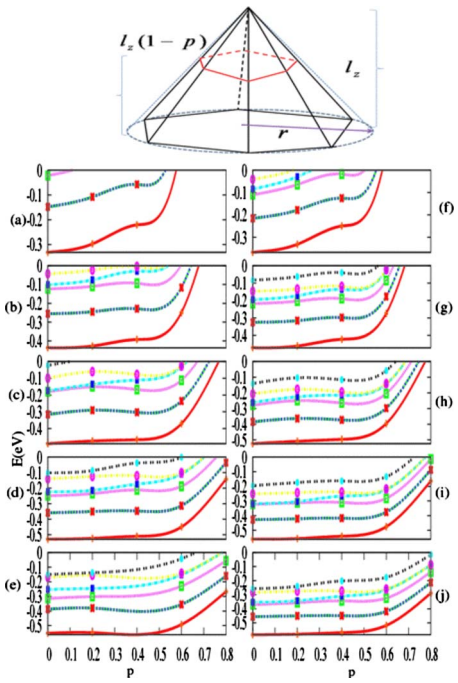

FIG. 4. (Color online) Energy of the ground and first electronic states with respect to the potential barrier for the square base pyramid with dimensions of 16×16 nm^2 and heights of 4 (a), 6 (b), 8 (c), 10 (d), and 12 nm (e), and with dimensions of 20×20 nm^2 and heights of 4 (f), 6 (g), 8 (h), 10 (i), and 12 nm (j). p is the truncating parameter of the pyramid height $l_z\cdot(1-p)$ ($p=0$, pyramid without truncation). In the upper panel the truncated pyramidal QD is represented. The pyramid base is a polygon with n edges ($n=3$ triangular, =4, square, =5 pentagonal, =6 hexagonal, etc). The truncated pyramid has a height$(1-p)\cdot l_z$, where l_z the height of the original pyramid and p is the truncating parameter.

cated pyramid (Fig. 4) where the base is a polygon with n edges ($n=3$ triangular, =4 square, =5 pentagonal, =6 hexagonal, etc). The truncated pyramid has a height$(1-p)\cdot l_z$, where l_z is the height of the original pyramid and p is the truncating parameter.

The confined states of the electrons are shown for different sizes of the InAs/GaAs QD pyramidal shape as a function of the truncation percentage p in Fig. 4. In a similar way to what happens with the truncated tetrahedron QD, the number of confined states decreases with the size and truncation percentage. The energy order from lower to higher energy (pyramidal QD) of the electron states is $a_1,e,a_1,a_2,a_1,a_1,e,\ldots$.

In Fig. 5 the first allowed transitions for a truncated pyramidal QD with a square base of 20 nm and different heights as a function of the parameter p are shown. According to Table I, the first transitions for z polarization are from electron level a_1 to hole level a_1 ($a_1\rightarrow a_1$) and from the electron level e to hole level e ($e\rightarrow e$). When p increases, the two transitions increase their energy and decrease their distance in energy. Furthermore, when the pyramid height increases, the energy of the two transitions decreases and their energy distance increases.

From Fig. 5, it is clear that a transition can be assigned to several truncated geometries. For example, a transition for 0.8 eV can be assigned to a transition $e\rightarrow e$ for $p=0.40$ and $h=8$ nm, $a_1\rightarrow a_1$ for $p=0.57$ and $h=6$ nm, $a_1\rightarrow a_1$ for $p=0.65$ and $h=8$ nm, and $a_1\rightarrow a_1$ for $p=0.80$ and $h=14$ nm.

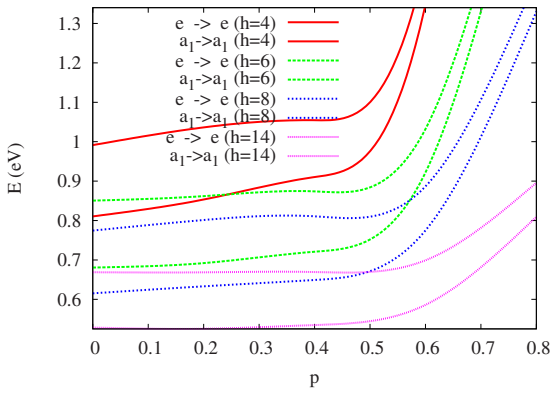

FIG. 5. (Color online) Energy of the first allowed transitions ($a_1\rightarrow a_1$ and $e\rightarrow e$, according to Table I) for a truncated pyramidal-shaped QD with square base of 20 nm and heights of 4, 6, 8, and 14 nm as a function of the truncating parameter p. For the hole levels the parameterization G has been used: $V_{B,h}^{(G)}=0.316$ eV and $m_{\mathrm{QD},h}^{(G)}=0.34m_0$ (Ref. 22). The transition with lower energy for each height corresponds to the $a_1\rightarrow a_1$ transition.

With just this information it is very difficult to characterize the size and shape of a sample with pyramidal QD with a square base. On the other hand, the structural techniques provide information on the size. Therefore, with the combination of both methods it is possible to characterize the QD present in the samples with greater accuracy.

Our results compare well with other results[24] where an eight-band $k\cdot p$/configuration interaction model calculations have been used for truncated pyramidal InAs/GaAs QDs with bases of 10.2 and 13.6 nm. The differences in energy of the ground and the first excited electronic state are lower than 0.1 eV.

C. Icosidodecahedral shape QD

Finally, we have obtained the energy levels of an InAs/GaAs QD with shape of an icosidodecahedron in order to show the versatility of the methodology used with respect to the shape of the QD. The icosidodecahedron has the symmetry of the icosahedra group I_h. The icosidodecahedron,[25] an archimedean solid, is a quasiregular polyhedron with 32 faces (20 triangular and 12 pentagonal), 30 identical vertices, and 60 identical edges.

In Fig. 6 the first electron energy levels for three icosidodecahedrons with different sizes are shown. As before, if the dot size increases, the electron energy level decreases. Conversely, if the dot size decreases, the electron energy level increases.

III. CONCLUSIONS

Extensive information about electron and hole confined InAs/GaAs QD levels and their spectrum is provided using on a model valid for arbitrarily shaped QD. This model is based on constant effective mass and constant potentials of the barrier and QD material. In this model the symmetry is used in order to obtain a better description of the QD and to reduce the computational cost. The spectrum is obtained in accordance with selection rules, which depend on the symmetry of the QD.

Downloaded 26 Jun 2013 to 128.42.202.150. This article is copyrighted as indicated in the abstract. Reuse of AIP content is subject to the terms at: http://jap.aip.org/about/rights_and_permissions

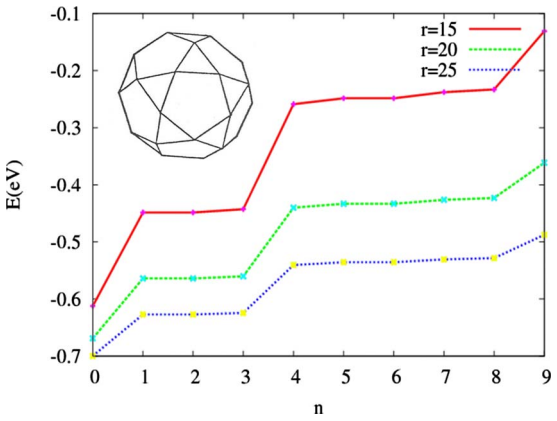

FIG. 6. (Color online) Energy of the firstly electron energy levels, labeled with index n, of the icosidodecahedron QD imbedded in spheres of 15, 20, and 25 nm.

From the results, the energy level structure of dots mainly depends on the shape more than the size. Thus, a direct comparison of calculated energy levels for a given size and shape with experimental spectroscopy and transport data is difficult. There are many possibilities of QD shapes which can correspond to an experimental spectrum. The changes in the electron effective mass and the change in the dot size also give similar qualitative results. Therefore, the results presented in this work can be useful for the analysis of samples as a complement to structural techniques.

ACKNOWLEDGMENTS

This work has been supported by the GENESIS FW project of the National Spanish program CONSOLIDER (CSD2006-0004), by the European Commission through the funding of the project IBPOWER (Grant Agreement No. 211640), and by La Comunidad de Madrid through the funding of the project NUMANCIA (Ref. No. S-0505/ENE/0310).

[1]M. H. Baier, E. Pelucchi, E. Kapon, S. Varoutsis, M. Gallart, I. Robert-Philip, and I. Abram, Appl. Phys. Lett. **84**, 648 (2004).
[2]G. S. Pearson and D. A. Faux, J. Appl. Phys. **88**, 730 (2000).
[3]Q. Xie, A. Madhukar, P. Chen, and N. P. Kobayashi, Phys. Rev. Lett. **75**, 2542 (1995).
[4]A. A. Darhuber, V. Holy, J. Stangl, G. Bauer, A. Krost, F. Heinrichsdorff, M. Grundmann, D. Bimberg, V. M. Ustinov, P. S. Kopev, A. O. Kosogov, and P. Werner, Appl. Phys. Lett. **70**, 955 (1997).
[5]N. N. Ledentsov, V. A. Shchukin, M. Grundmann, N. Kirstaedter, J. Böhrer, O. Schmidt, D. Bimberg, V. M. Ustinov, A. Yu. Egorov, A. E. Zhukov, P. S. Kopev, S. V. Zaitsev, N. Yu. Gordeev, Zh. I. Alferov, A. I. Borovkov, A. O. Kosogov, S. S. Ruvimov, P. Werner, U. Gösele, and J. Heydenreich, Phys. Rev. B **54**, 8743 (1996).
[6]Y. Androussi, T. Banabbas, and A. Lefebvre, Philos. Mag. Lett. **79**, 201 (1999).
[7]D. Leonard, K. Pond, and P. P. Petroff, Phys. Rev. B **50**, 11687 (1994).
[8]T. Benabbas, P. Francios, Y. Androussi, and A. Lefebvre, J. Appl. Phys. **80**, 2763 (1996).
[9]P. W. Fry, I. E. Itskevich, D. J. Mowbray, M. S. Skolnick, J. J. Finley, J. A. Barker, E. P. O'Reilly, L. R. Wilson, I. A. Larkin, P. A. Maksym, M. Hopkinson, M. Al-Khafaji, J. P. R. David, A. G. Cullis, G. Hill, and J. C. Clark, Phys. Rev. Lett. **84**, 733 (2000); I. Kegel, T. H. Metzger, P. Fratzl, J. Peisl, A. Lorke, J. M. García, and P. M. Petroff, Europhys. Lett. **45**, 222 (1999); P. B. Joyce, T. J. Krzyzewski, G. R. Bell, B. A. Joyce, and T. S. Jones, Phys. Rev. B **58**, 15981 (1998).
[10]G. Lamouche and Y. Lepin, Phys. Rev. B **51**, 1950 (1995); M. Peeters and V. A. Schweigert, *ibid.* **53**, 1468 (1996).
[11]A. Wojs, P. Hawrylak, S. Fafard, and L. Jasak, Phys. Rev. B **54**, 5604 (1996); A. H. Rodriíguez, C. Trallero-Giner, S. E. Ulloa, and J. Mariín-Antu a, *ibid.* **63**, 125319 (2001).
[12]Ph. Lelong and G. Bastard, Solid State Commun. **98**, 819 (1996); D. M. T. Kuo and Y. C. Chang, Phys. Rev. B **61**, 11051 (2000).
[13]P. C. Sercel and K. J. Vahala, Phys. Rev. B **42**, 3690 (1990); L. Rosen and M. Rosen, *ibid.* **58**, 7120 (1998); N. Singh, V. Ranjan, and V. A. Singh, Int. J. Mod. Phys. **14**, 1753 (2000).
[14]M. Grundmann, O. Stier, and D. Bimberg, Phys. Rev. B **59**, 5688 (1999); A. J. Williamson and A. Zunger, *ibid.* **59**, 15819 (1999); C. Prior, *ibid.* **60**, 2869 (1999); M. Califano and P. Harrison, *ibid.* **61**, 10959 (2000); J. Shumway, L. R. C. Fonseca, J. P. Leburton, R. M. Martin, and D. M. Ceperley, Physica E (Amsterdam) **8**, 260 (2000).
[15]S. S. Li and J. B. Xia, J. Appl. Phys. **84**, 3710 (1998); M. Califano and P. Harrison, *ibid.* **88**, 5870 (2000).
[16]C. Tablero, J. Chem. Phys. **122**, 064701 (2005).
[17]L. He and A. Zunger, Phys. Rev. B **73**, 115324 (2006).
[18]V. Popescu, G. Bester, and A. Zunger, Appl. Phys. Lett. **95**, 023108 (2009).
[19]C. Daengngam and T. Pengpan, Eur. J. Phys. **26**, 1139 (2005).
[20]Y. Li, O. Voskoboynikov, C. P. Lee, S. M. Sze, and O. Tretyak, J. Appl. Phys. **90**, 6416 (2001); Y. Li, O. Voskoboynikov, C. P. Lee, and S. M. Sze, Comput. Phys. Commun. **141**, 66 (2001).
[21]V. A. Fonoberov, E. P. Pokatilov, V. M. Fomin, and J. T. Devreese, Phys. Rev. Lett. **92**, 127402 (2004).
[22]M. Grundmann, O. Stier, and D. Bimberg, Phys. Rev. B **52**, 11969 (1995); M. Grundmann, N. N. Ledentsov, O. Stier, D. Bimberg, V. M. Ustinov, P. S. Kopev, and Z. I. Alferov, Appl. Phys. Lett. **68**, 979 (1996).
[23]M. A. Cusack, P. R. Briddon, and M. Jaros, Phys. Rev. B **54**, R2300 (1996).
[24]R. Heitz, F. Guffarth, K. Pötschke, A. Schliwa, and D. Bimberg, Phys. Rev. B **71**, 045325 (2005).
[25]R. Williams, *The Geometrical Foundation of Natural Structure: A Source Book of Design* (Dover, New York, 1979).

Downloaded 26 Jun 2013 to 128.42.202.150. This article is copyrighted as indicated in the abstract. Reuse of AIP content is subject to the terms at: http://jap.aip.org/about/rights_and_permissions